Microfabricated, Combustion-Driven Jet Actuators for Flow Control Applications

T. Crittenden and A. Glezer
Woodruff School of Mechanical Engineering
801 Ferst Drive N.W.

E. Birdsell and M. Allen
School of Electrical and Computer Engineering
777 Atlantic Drive N.W.
Georgia Institute of Technology, Atlanta, GA, USA 30332

Abstract

A high-power small-scale combustion-based fluidic actuator is developed for aerodynamic control of high-speed flows. The actuator produces a momentary high velocity jet from an exhaust orifice by the ignition of premixed fuel and oxidizer in a small (cm^3 scale) combustion chamber as shown in figure below. The flow into the chamber is regulated using a fluidic element without moving parts. The performance of the actuator (in terms of time-dependent chamber pressure and thrust) is extensively characterized over a range of operational parameters including fuel type and mixture ratio, orifice diameter, combustor volume, and mixture flow rate. The combustion process typically lasts on the order of 1 to 5 ms and chamber pressures of up to 5 atmospheres are achieved and produce sonic speeds at the jet orifice. Operating frequencies greater than 150 Hz have been realized. The effectiveness of these actuators for transient, controlled reattachment of the flow over a stalled airfoil in demonstrated in low-speed wind tunnel experiments. Arrays of such jets that can be integrally mounted into large aerodynamic surface are developed for external aerodynamic flow control in applications using MEMS-based batch fabrication techniques. Actuator arrays have been created using alumina ceramic laminates and patterning is performed using a high-power Nd:YLF laser, which integrally defines the combustion chamber volume, exhaust orifice, and rectangular pathways for fuel/air mixing, flow into the chamber, and pressure sensor attachment. Screen printing techniques are used to create surface-mounted platinum electrodes for ignition. The ceramic combustion chambers have been tested with results generally similar to those for conventionally fabricated combustors.

I. Introduction

Controlled reattachment of separated flows over lifting surfaces at moderate and high angles of attack with the objective of improving aerodynamic performance and extending the flight envelope has been the focus of a number of investigations since the early eighties. In recent years, active control techniques have achieved varying degrees of separation control by manipulation of the unstable separated free shear layer using pulsed blowing on the time scale of the flow about the airfoil thereby exploiting a Coanda-like effect for unsteady reattachment either at the leading edge (e.g., Chang et al.[1], McManus et al.[2], Seifert et al. 1996[3]), or near the flap hinge to increase its effectiveness (e.g., Seifert et al., 1993[4]). In these experiments, the excitation was typically applied at a dimensionless (reduced) frequency, $F^+ \sim O(1)$ such that that excitation period scaled with the time of flight over the length of the reattached flow.

A flow control approach that does not necessarily rely on coupling to a global flow instability has been demonstrated by Smith et al.[5] and Amitay et al.[6, 7] who used fluidic modification of the apparent aerodynamic shape of aero-surfaces by means of synthetic (zero net mass flux) jets for the suppression of separation over an unconventional airfoil at moderate Reynolds numbers (up to 10^6). The actuation is typically applied at frequencies that are at least an order of magnitude higher than the characteristic frequency of the base flow [e.g., $F^+ = O(10)$] resulting in a quasi-steady interaction domain between the jet and the cross flow. Recent experiments by Erk[8] demonstrated suppression of separation on an FX61-184 airfoil at Reynolds numbers up to $3 \bullet 10^6$ using synthetic jet actuation at frequencies up to $F^+ \sim O(100)$.

The earlier work on separation control has emphasized the utility of pulsed jet actuators having a (dimensionless) momentum coefficient on the order of 10^{-3}. While it is relatively simple to develop such actuators either for wind tunnel testing or for small-scale vehicles operating at relatively low speeds (e.g., UAVs), it is clear that pulsed jet actuation having similar (or even potentially higher) levels of momentum coefficient at higher flight speeds (e.g., transonic or supersonic) will require high speed actuator jets and different actuation hardware.

The present paper focuses on the development of a novel, high-powered actuator, which uses a combustion process to drive a high velocity exhaust jet. Section II describes the basic actuator concept, with section III reviewing the fundamental parameters and limitations of combustion on the scale envisioned. Section IV details the results of the basic investigation of the actuator performance (primarily through dynamic combustor pressure measurements), varying parameters such as fuel type and mixture ratio (Φ), exhaust orifice diameter (d), chamber volume (V), and mixture flowrate (Q). Section V presents the initial flow control results focusing on transient reattachment of separated flows. Finally, Section VI discusses microfabrication techniques used to create arrays of combustion actuators using batch processing.

II. The Combustion-Driven Jet Actuator Concept

Combustion-driven fluidic actuation yields a high momentum jet by exploiting the chemical energy of gaseous fuel/air mixture. The basic element of the system is, essentially, a fluidic amplifier where a low volume flow rate premixed fuel having relatively low momentum fills a small (O ~ 1 cc) arbitrary-shape combustion chamber bounded by an orifice plate as shown schematically in Figure 1. A spark (or other ignition source) ignites the mixture, creating a high pressure burst within the combustor and a subsequent jet emanating from one or more exhaust orifices. At the scales envisioned, the entire combustion process is complete within several milliseconds and the cycle resumes with fresh fuel/oxidizer mixture entering the chamber and displacing the remaining combustion products. The period of the system (τ) is limited by the duration of the high pressure pulse (t_{pulse}) and the chamber refill time (t_{refill}). Note that such devices can be operated in a non-premixed mode, in which an additional characteristic mixing time (t_{mix}) must also be included in the cycle period. The cycle frequency is continuously variable and is controlled by the spark/ignition source and the refill flow rate. For a 1 cc combustor, operating frequencies in excess of 150 Hz may be achieved using hydrogen/air mixtures.

The flow of reactants into the chamber can be regulated by one of several means. One option is to include small-scale (possibly MEMS-based) electronic valves, which can be timed to open during the refill phase and close during the combustion process and therefore allow precise timing control of the combustion and refill processes. Other options utilize either passive mechanical or fluidic valves which respond to and are driven by the increased pressure within the combustion chamber although with reduced operation timing and speed control. Unlike electronic valves, passive valves require a minimum chamber pressure to operate properly and ensure that the inflow of reactants stops after the combustion process begins. The current configurations are based on passive valves for regulation. Therefore, the only power and electronics infrastructure requirement is for the ignition source. An important feature of this design is that these actuators can be fabricated in low-weight, individually addressable arrays that can be operated over a broad frequency range. Because of the flexibility of the shape of the combustion chamber, actuator arrays can be conformed and integrated into surfaces of arbitrary shapes.

III. Small-Scale Combustion

A critical limit of small-scale combustion is the heat transfer from the hot combustion gases to the walls of the combustion chamber. When the energy loss due to heat transfer to the walls is greater than the energy generated by the combustion process, the flame may be extinguished. For a given flow, the characteristic scale associated with this extinction process is known as the quenching distance, which is the critical dimension for a given configuration (typically tube diameter or distance between parallel plates) where a flame extinguishes rather than propagates. For stoichiometric, quiescent mixtures of hydrogen/air and propane/air at STP, the quenching distance between parallel plates is 0.64 mm and 2.0 mm, respectively[9]. The quenching distance is a function of both mixture ratio and initial pressure, and typically increases with mixture ratios off stoichiometric and decreases with higher initial pressure[10]. Thus, these quenching distances may be considered the absolute lower limits on chamber dimensions to insure combustion at STP, as well as setting a preferred minimum spark gap for ignition. Combustion in smaller dimensions can be achieved by pressurizing the gas prior to ignition, thus increasing the chemical energy release for a given volume of mixture. A number of applications that use this approach include MEMS-based power generation devices[11] and small-scale engines used for powered models.

The combustion-powered jet actuator only allows minimal pre-pressurization since the system is constantly open to the atmosphere at the exhaust. Small-scale combustion near atmospheric pressure has not been investigated extensively. Recently, Faulkner, et al.[12] investigated ignition and flame propagation in closed combustors having high surface area-to-volume ratio using propane/air mixtures. Successful combustion was demonstrated in cross sectional height as small as 3.1 mm. The peak chamber pressure and duration of the pressure pulse were directly related to the volume to surface area ratio such that higher volume per unit surface area produced higher pressure peaks.

The essential parameters affecting the small-scale combustion process within the present jet actuator are the fuel and mixture ratio (which affect the chemical energy available per unit volume and the chemical reaction rate), exhaust orifice diameter (controlling the rate at which gas is vented from the combustor), chamber volume, and mixture flow rate (affecting the gas velocities and turbulence intensity within the combustor). Other secondary factors affecting the combustion process include the wall surface area and the temperature of the combustor walls, which affect the heat transfer losses and radical quenching effects (not addressed in the present text, but an object of ongoing study). It is noteworthy the flame temperature (approximately 2400K) is *always* much higher than the typical wall temperature (within present material limits) and therefore the heat losses are virtually invariant.

IV. Actuator Performance

The baseline test actuation device has conventionally fabricated interchangeable aluminum combustion chambers, cylindrical in shape varying volume and aspect ratio. Orifice plates of varying diameters are attached to the top of the chambers holding the orifice plate thickness at double the orifice diameter (l/d=2.0). Fuel and air are premixed upstream of the actuator using thermal mass flowmeters with metering valves. The mixture is then fed through a passive fluidic element into the combustion chamber underneath the exhaust orifice. For most experiments, the mixture is ignited with a spark produced by a modified automotive ignition system with a nominal energy level of 50 mJ. The duration (and energy) of the spark are controlled by the trigger pulse width and, depending on the gap size, can be varied between 120 μs and approximately 2 ms. Spark gaps of 1 and 2 mm are used for hydrogen and propane, respectively. While in the present work hydrogen and propane are the primary fuels, acetylene and other gaseous fuels have also been demonstrated as viable options.

The time-dependent pressure within the chamber is measured using an Endevco piezoresistive high-temperature pressure transducer that is mounted into the wall of the chamber and sampled at a frequency of 100 kHz. Schlieren images of the flow are recorded using a standard CCD camera with a single-pass Schlieren visualization system. Flame photography is obtained using a cubical 1 cc combustor having a pyrex side wall. The spark trigger signal is recorded and used to provide timing and phase data for all measurements. All visualization images (photography or Schlieren) use the video vertical sync signal from the CCD camera as a timing master to trigger the spark and thus provide phase-locked imaging (which limits the visualization runs to frequencies of either 30 Hz or its submultiples).

Phase-averaged (time-dependent) pressure traces measured within a V = 1 cc cylindrical (H/D = 1.27) combustion chamber with d = 1.30 mm exhaust for various mixtures of air and hydrogen or propane are shown in Figure 2. (The pressures here and throughout are presented as the pressure ratio between the combustor and atmospheric pressure, P_r, and are referenced to the beginning of the spark ignition at t = 0 ms.) The experiments are limited to stoichiometric and fuel-lean mixtures ($\Phi \leq 1$) as it is assumed desirable to minimize fuel consumption for the actuator. In general, due to differences in flame propagation speeds, the hydrogen mixture exhibits substantially shorter pressure pulses with faster characteristic rise time and higher peak pressures than propane. For laminar flames, the respective propagation speeds in stoichiometric (Φ = 1) hydrogen and propane air mixtures are 210 cm/s and 44 cm/s[11], respectively, with subsequent reductions in flame speed for leaner mixtures of both. The pressure curve trends match the trends for laminar flame speed, with mixtures with lower flame speeds exhibiting longer pressure pulses and lower peak pressures. This is not unexpected as the flame speed effectively determines the rate of release of chemical energy and the resulting pressure rise time. Also of note are the substantially wider flammability limits of hydrogen (down to Φ= 0.5) compared to propane (Φ= 0.8). The literature lists both fuels with slighter wider flammability limits at STP, but attempts to burn at mixture ratios lower than those shown yielded a sputtering, incomplete combustion process without discernable pressure rise in the chamber.

Results for variation in orifice diameter are presented in Figure 3 for stoichiometric mixtures of both hydrogen and propane in a 1 cc combustor. As expected, larger d values result in lower peak pressures and shorter pulse durations owing to faster venting of the high-pressure gas within the chamber. The rise time of the pressure pulse to the peak pressure (t_{peak}) is largely invariant with orifice diameter, suggesting that the combustion process within the chamber is largely unaffected by the exhaust orifice size. The effect of variation in chamber volume for hydrogen-air (Φ= 1.0) with d = 1.30 mm is shown in Figure 4 for V = 0.25, 0.5, 1.0, 1.5, and 2.0 cc (all with H/D = 1.27). These data show that for a fixed orifice size, the peak pressures and burn times decrease as the chamber volume is decreased. A slightly faster pressure rise is observed for smaller volumes, as the burned region within the chamber occupies a higher percentage of the total volume in the initial flame propagation. For the lowest volume (V = 0.25 cc), the entire combustion process is complete in just under 1 msec with still sufficient pressure to generate sonic velocities at the orifice ($P_r \geq 1.89$).

The results discussed so far have all been for the baseline mixture flow rate (Q) of 10 cc/s for a 1.0 cc combustor (with Q scaled proportionally with the volume for other volumes tested). The flow rate must be increased to allow increasing actuation frequencies, resulting in both increased mean flow velocities within the chamber and increases in turbulence intensity. The combustor pressures varying the flow rate (up to 100 cc/s) while holding the mixture ratio and orifice diameter constant for a V = 1.0 cc chamber are shown in Figure 5. A sharp increase in the pressure peak may be observed with decreases in the pulse duration. This is due to increased turbulence within the chamber effectively increasing the flame propagation speed (similar to the effects for increasing mixture ratio.) Similar behavior occurs for propane mixtures. Some features of the flame propagation are captured in a sequence of images of the flame within the chamber during the combustion cycle (Figure 6). The images are for stoichiometric propane/air mixture in a 1 cm^3 chamber with a 1.27 mm orifice and Q = 75 cc/s (photography of hydrogen flames was not possible as light emission from hydrogen is almost entirely in the ultraviolet and can not be visualized with standard camera equipment). The chamber is oriented such that the refill gas enters at the bottom and the exhaust orifice is located at the top. The mean gas motion within the chamber results in forward arcing of the spark as shown in Figure 6a

(0.5 ms following the ignition trigger). These images show that the flame also follows the mean flow and initially propagates towards the top of the chamber with substantial wrinkling of the flame front. However, as the cycle progresses and the pressure increases the flow of fuel/air mixture into the chamber is cut off, allowing the flame to turn and spread to the bottom of the chamber.

A sequence of phase-locked Schlieren images of the ejected jet during the combustion cycle is shown in Figure 7 relative to the pressure time-history of hydrogen-air ($\Phi = 0.7$) combustion in a 1 cc chamber with d = 1.30 mm, Q = 50 cc/s, and f = 30 Hz. The images are taken at t = 0.44, 0.70, 1.2, 2, 3, and 4.8 ms using a 125 μs shutter speed, and the streamwise field of view is approximately 25 orifice diameters. Within the combustion cycle, the jet speed downstream of the exit plane varies from subsonic to supersonic and then becomes subsonic again before it decays when the combustor pressure is atmospheric (within approximately 3 msec). The jet flow in the far field is highly turbulent as is evidenced by the level of small-scale structures. An enlarged view of the flow near the jet exit plane at 0.7 ms (near the peak pressure) suggests the presence of a cellular shock structures within approximately 5 orifice diameters (6 mm) downstream from the jet exit plane. Although this image is somewhat smeared due to the fluid motion and the variation in combustor pressure during the shutter opening time, their appearance coincides with the period in which the pressure level is sufficient to generate sonic speed at the orifice. Note that when the refill of the combustor begins (approximately 4 ms following the ignition spark), a weak starting vortex followed by a weak jet of combustion products (remnants from the cycle that is just completed) appear near the jet exit plane.

V. Separation Control Experiments

For flow control experiments, a bank of 8 combustion actuators were integrated into the leading edge of a constant section, 21.5 cm chord (c), 17.4 cm span active wing section. The airfoil section used for the wing is a proprietary design and thus is not presented in its entirety here. A notable feature of the airfoil section is that it has a relatively sharp leading edge. The leading radius is approximately 0.016c. This contributes to large scale flow separation from the leading edge of the wing for this configuration as will be shown. The combustion actuator chambers were each 1.4 cm wide and of triangular cross-section (to allow integration into the sharp leading edge) with 1.7 cm length and 0.7 cm height (V = 0.85 cc each). The exhaust orifice of the actuator was a slot 1.4 cm wide by 0.15 mm high, directed normal to the wing in the upstream direction at the leading edge. Premixed fuel delivery lines and spark wires were fed from the side of the model through dummy wing sections spanning the remaining width of the wind tunnel, separated from the active section by fences. In all the results presented the actuators were run synchronously, to create as close to a uniform 2-D flowfield as possible across the active section.

The wing was mounted in an open-return, low-speed wind tunnel having a square test section measuring 91 cm on a side. The maximum tunnel velocity is 30 m/s with a free-stream turbulence level less than 0.15%. The upper and lower walls of the wind tunnel are adjusted to compensate for blockage created by the wing. The nominally two-dimensional flow field is computed from a sequence of PIV images that are captured in the x-y plane above the suction side of the airfoil. Each PIV data set is comprised a frame measuring 150mm on the side where time- or phase-averaged velocity (and vorticity) distributions are computed from an ensemble of 125 image pairs. The illumination is provided by a pair of 120mJ Nd:Yag lasers with a maximum repetition rate of 15Hz. The laser sheet is formed using standard optical arrangement, and the images are captured using a 1008x1016-element dual frame CCD camera mounted on a two-axis traverse.

A progression of smoke flow visualization images of the airfoil mounted at a high angle of attack ($\alpha = 24.1^{\circ}$) are presented in Figure 8 with a freestream velocity (U_∞) of 12.5 m/s ($Re = 1.95\times10^5$) showing a single pulse from the bank of actuators and its transient effect on the flow field. Figure 8a is taken before the pulse and provides a baseline for the flow, indicating broad flow separation occurring at the leading edge. The images in 8b and 8c (t = 1 and 3 msec, respectively) cover the entire duration of the high pressure pulse within the chamber (and subsequent exhaust jet). Over this period, the jet may be seen exiting the leading edge of the airfoil as a darkened region in the otherwise seeded flow. By 3 msec, no more jet is visible at the leading edge although a small vortical structure has developed as a result of this high velocity jet being turned back on itself by the freestream flow. The remainder of the images show this vortical structure growing as it progresses back over the airfoil surface at roughly 50% of the freestream velocity, following the trajectory of the shear layer established in the baseline separated flow. Behind this structure, the flow exhibits a transient reattachment to the airfoil surface before subsequently returning to the broadly separated state.

Figure 9 shows PIV data including velocity vectors and vorticity contours for the same flow conditions, but with an actuation frequency of 45 Hz (St = 0.82 based on the chord length), progressing from just after ignition (t/τ = 0.045) to just before the next actuator pulse (t/τ = 0.900). In this case, the final image provides some idea of the baseline of the flow, indicating nearly continuous flow attachment to the surface of the airfoil, with only a slight recirculation bubble visible near the surface. The actuator pulse shows the same type of development as for the transient case, with the structure clearly visible from the vorticity contours. Again the vortex rolls backward following the shear layer of the flow (in this case, very near the upper surface of the airfoil). In doing so, it strengthens the flow attachment to an effectively complete reattachment (see t/τ = 0.675). As the next cycle approaches the separation begins to develop again, with the recirculation region growing from the leading edge of the airfoil backwards. Test at several frequencies indicate that as St is increased, the degree of separation continuously decreases to essentially constant attachment near St = 1.

VI. Combustion Chamber Microfabrication

Ultimately, it is desirable to be able to create arrays of combustion-based actuators with integrated fluidic piping for fuel and air and integrated electrodes for initiation of combustion. MEMS technology (microelectromechanical systems) offers an attractive approach to realize such structures in a batch-fabrication-compatible manner. When considering appropriate materials for pulse combustor fabrication, alumina ceramic laminates are attractive, e.g., due to their relatively low thermal conductivity. Furthermore, the patterning (e.g., by lasers) of ceramic laminate greensheet and subsequent batch fabrication of ceramic parts by means of large area lamination and dicing has been demonstrated industrially by the electronic packaging industry[13]. This approach is also suitable for micromachining; e.g., it has been recently exploited to fabricate micromachined pressure sensors[14]. Lamination-based approaches, such as this work as well as silicon-fusion-bonding approaches[15], allow for the incorporation of fluidic pathways within the combustor. Finally, conductor inks that are thermal-expansion-matched to the alumina are available for the integration of any required electrical functionality, such as spark plugs or valve addressing.

In the present work, a radial four combustor array composed of alumina ceramic alumina with integrated spark pads and fluid passages is demonstrated. The ceramic chamber is constructed from multiple laminate layers of commercially available Al_2O_3 sheets which are patterned using a 12 watt 1048nm Nd:YLF laser (die stamping of the individual layers is also a feasible approach). Figure 10 illustrates the design concept and shows the individual chamber layers after laser patterning. Rectangular channels for intake and exhaust are formed in the planar direction. A platinum electrode on the inner wall of the combustion chamber provides an ignition source, and is fabricated by screen-printing platinum ink on one of the chamber end-caps. Before final assembly, the screen-printed electrode and its substrate are sintered, typically at 900^{o}C for 4 hours, to cure the platinum ink. Individual layers are stacked using alignment pins to ensure accurate positioning of the multilayer structure during the curing process, and are either pressure-laminated and sintered or may be adhesively bonded to form the final combustion chamber. The final combustor array is shown in Figure 11 with an inset showing the slot exhaust orifice for a single chamber. Although this particular design was not instrumented with a pressure transducer, previous tests have demonstrated nearly identical pressure curves for combustors created using this technique as compared to conventionally fabricated combustors of similar geometric properties (volume, cross-section, etc.)[12]. Figure 11 also includes a single Schlieren image of the exhaust jet from the combustion process within one of these combustors.

VI. Conclusions

A novel fluidic actuator for flow control has been demonstrated which utilizes a small-scale combustion chamber to create a pulsed high velocity jet of exhaust gases. The pressure rise within the actuator and the subsequent characteristics of the exhaust jet are controlled by the combustion properties within the chamber (set primarily by the fuel type and mixture ratio, the chamber volume and shape, and the mixture flow rate) and the rate at which gas is vented form the chamber (set by the exhaust orifice size). The pressure pulse duration is typically a few milliseconds with peak pressures up to 5 atmospheres recorded and combustion frequencies up to 150 Hz demonstrated. The combustion-driven jet actuator has been demonstrated for transient reattachment of separated flows at high angles of attack. Finally, the simple physical design of the actuator makes it particularly suitable for batch fabrication through MEMS-based approaches. In particular, ceramic combustor arrays have been fabricated and shown to be feasible.

References

1. Chang, R.C., Hsiao, F.-B., and Shyu, R.-N.,“ Forcing level effects of internal acoustic excitation on the improvement of airfoil performance,” J. of Aircraft, 29(5), p.823-829, 1992.

2. McManus, K.R., Ducharme, A., Goldey, C., and Magill, J., “Pulsed Jet Actuators for Suppressing Flow Separation,” AIAA Paper 96-0442, January 1996.

3. Seifert, A., Darabi, A., and Wygnanski, I., “Delay of airfoil stall by periodic excitation,” J. of Aircraft, 33(4), p. 691-698, 1996.

4. Seifert, A., Bachar, T., Koss, D., Shepshelovich, M., and Wygnanski, I., “Oscillatory Blowing: A Tool to Delay Boundary-Layer Separation,” AIAA Journal, Vol. 31, No. 11, p. 2052-2060, November 1993

5. Smith, D.R., Amitay, M., Kibens, V., Parekh, D.E., and Glezer, A., “Modification of lifting body aerodynamics using synthetic jet actuators,” AIAA Paper 98-0209.

6. Amitay, M., Kibens, V., Parekh, D.E., and Glezer, A., “Flow reattachment dynamics over a thick airfoil controlled by synthetic jet actuators,” AIAA Paper 99-1001.

7. Amitay, M., Smith, B.L., and Glezer, A., “Aerodynamic flow control using synthetic jet technology,” AIAA Paper 98-0208.

8. Erk, P.P., “Separation Control on a Post-Stall Airfoil using Acoustically Generated Perturbations”, Ph.D. Dissertation, Technische Universitat Berlin, Germany, 1997.

9. Turns, Stephen R., *An Introduction to Combustion: Concepts and Applications*, McGraw-Hill, Inc., New York, 1996.

10. Lewis B., and Von Elbe, G., *Combustion, Flames and Explosions of Gases*, 3rd Ed., Academic Press, Orlando, 1987.

11. Epstein, A.H., et al, “Power MEMS and microengines,” 1997 International Conference on Solid-State Sensors and Actuators, p.753-756, vol. 2, 1997.

12. Faulkner, J.C., Scarborough, D.E., and Jagoda, J.I., “A Study of Ignition and Flame Propagation in a Small, High Surface-To-Volume Ratio Combustor,” AIAA, Paper 2000-0591.

13. Tummala et al, “Microelectronics Packaging Handbook,” Chapman and Hall, New York, NY, 1997.

14. English et al., “Wireless Micromachined Ceramic Pressure Sensors,” Proc. MEMS ’99, 1999.

15. Mehra, Schmidt, et al., “Microfabrication of High Temperature Silicon Devices Using Wafer Bonding and Deep Reactive Ion Etching,” JMEMS, June 1999.

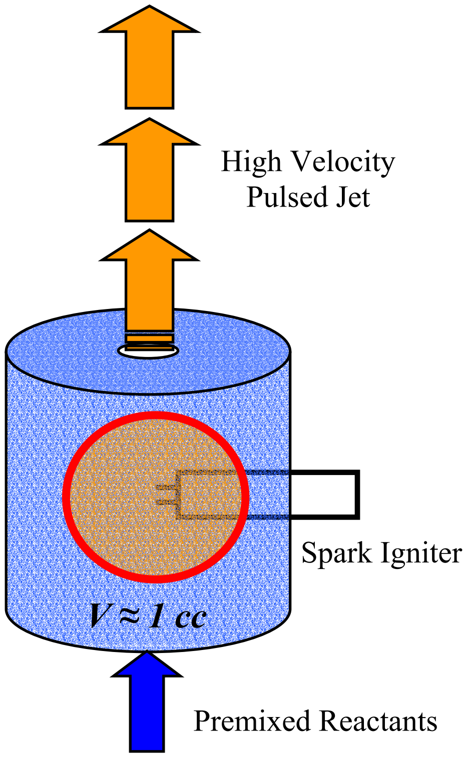

Figure 1. Schematic illustration of combustion-driven jet actuator

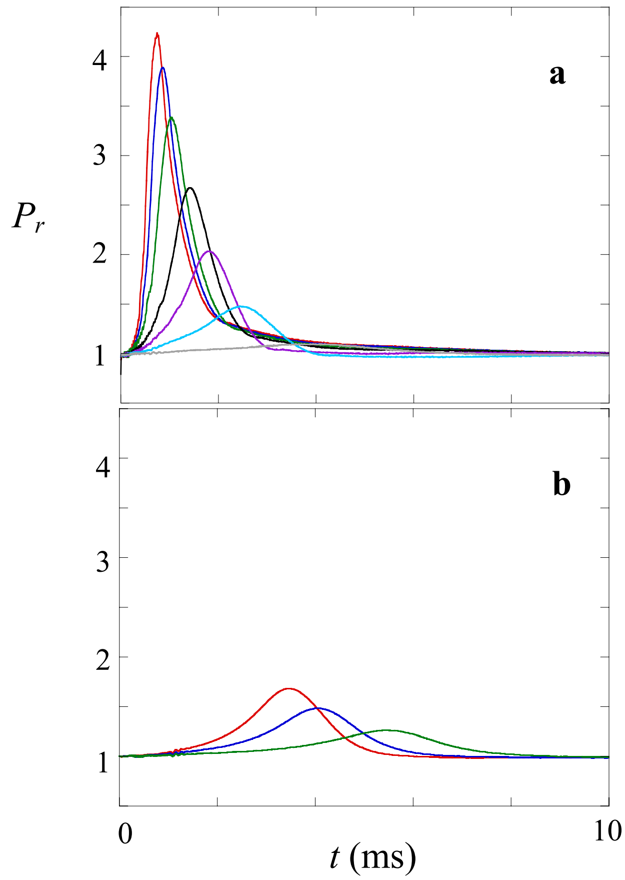

Figure 2. Phase averaged combustor pressure for d = 1.30 mm for a) hydrogen and b) propane varying mixture ratio for Φ = 1.0, 0.9, 0.8, 0.7, 0.6, 0.5, and 0.4.

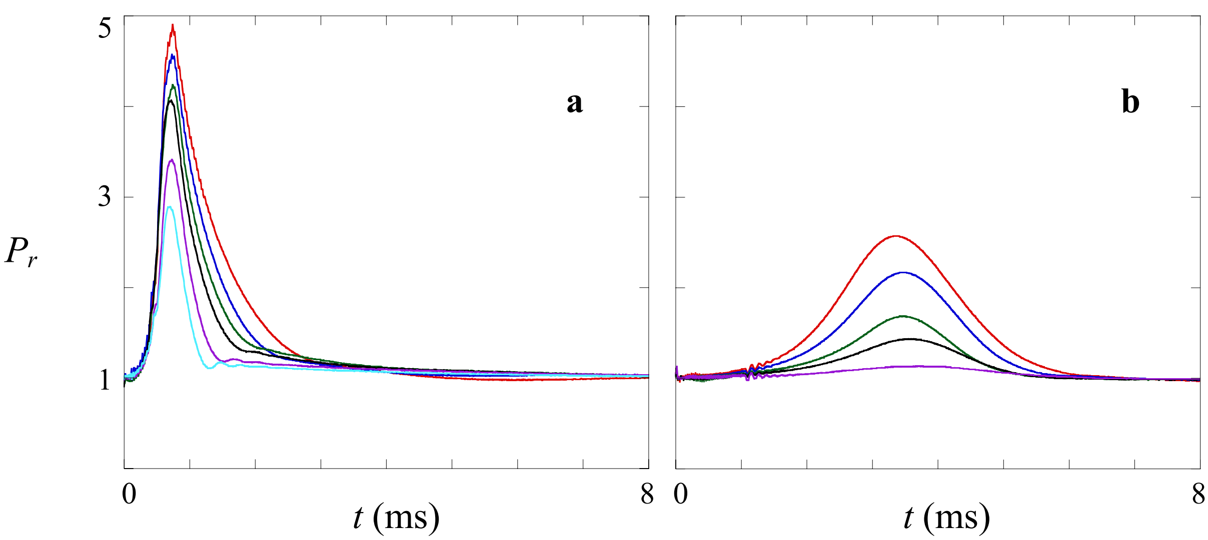

Figure.3. Phase averaged combustor pressure for Φ=1.0 for a) hydrogen and b) propane varying orifice diameter for d = 0.89, 1.09, 1.30, 1.50, 1.78, and 2.21 mm.

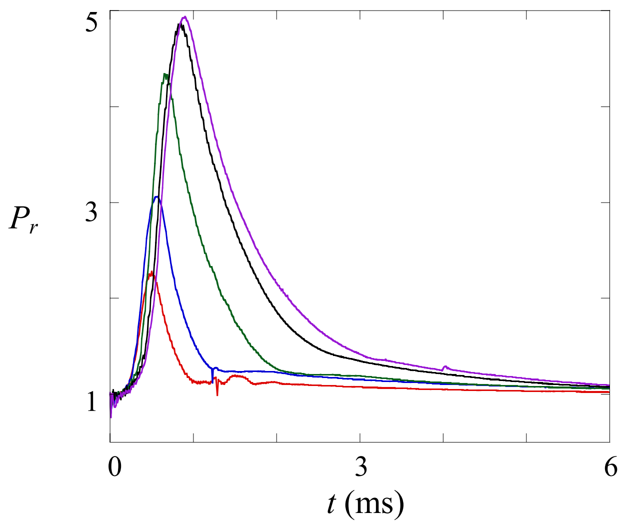

Figure 4. Phase averaged combustor pressure for hydrogen (Φ = 1.0) with d = 1.30 mm for V = 0.25, 0.50, 1.00, 1.50, and 2.00 cc.

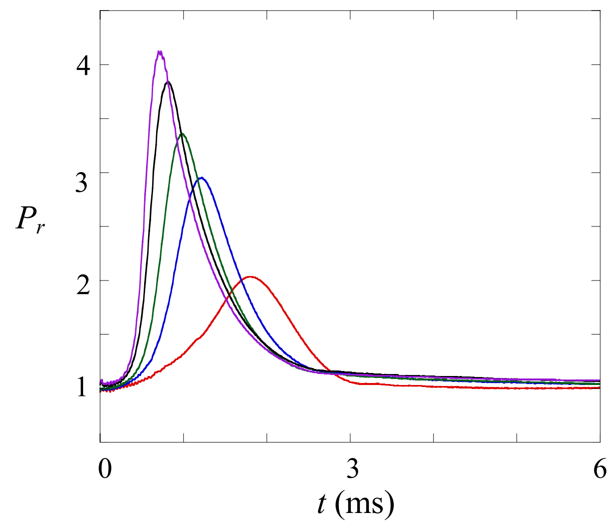

Figure 5. Phase averaged combustor pressure for hydrogen (Φ = 0.6) with d = 1.30 mm for Q = 10, 30, 50, 75, and 100 cc/s.

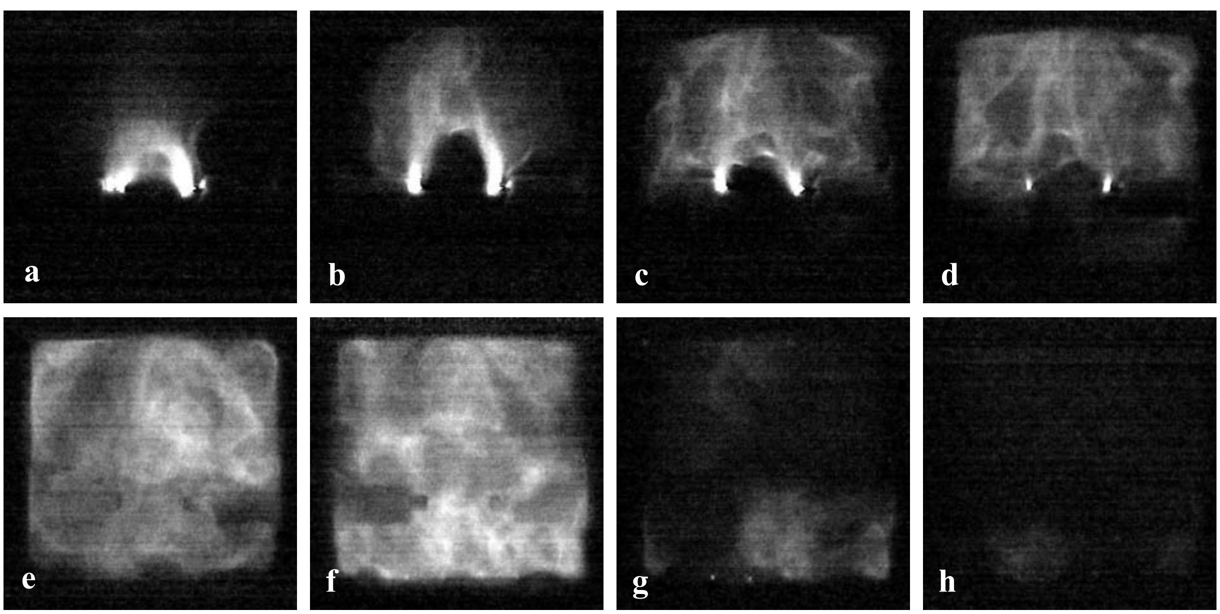

Figure 6. Sequence of flame photographs inside 1 cc (cubical) combustion chamber with d = 1.30 mm and stoichiometric propane/air mixture at t = 0.25 (a), 0.5 (b) 0.75 (c) 1.0 (d) 1.5 (e), 2.0 (f), 2.5 (g), and 3.0 (h) ms

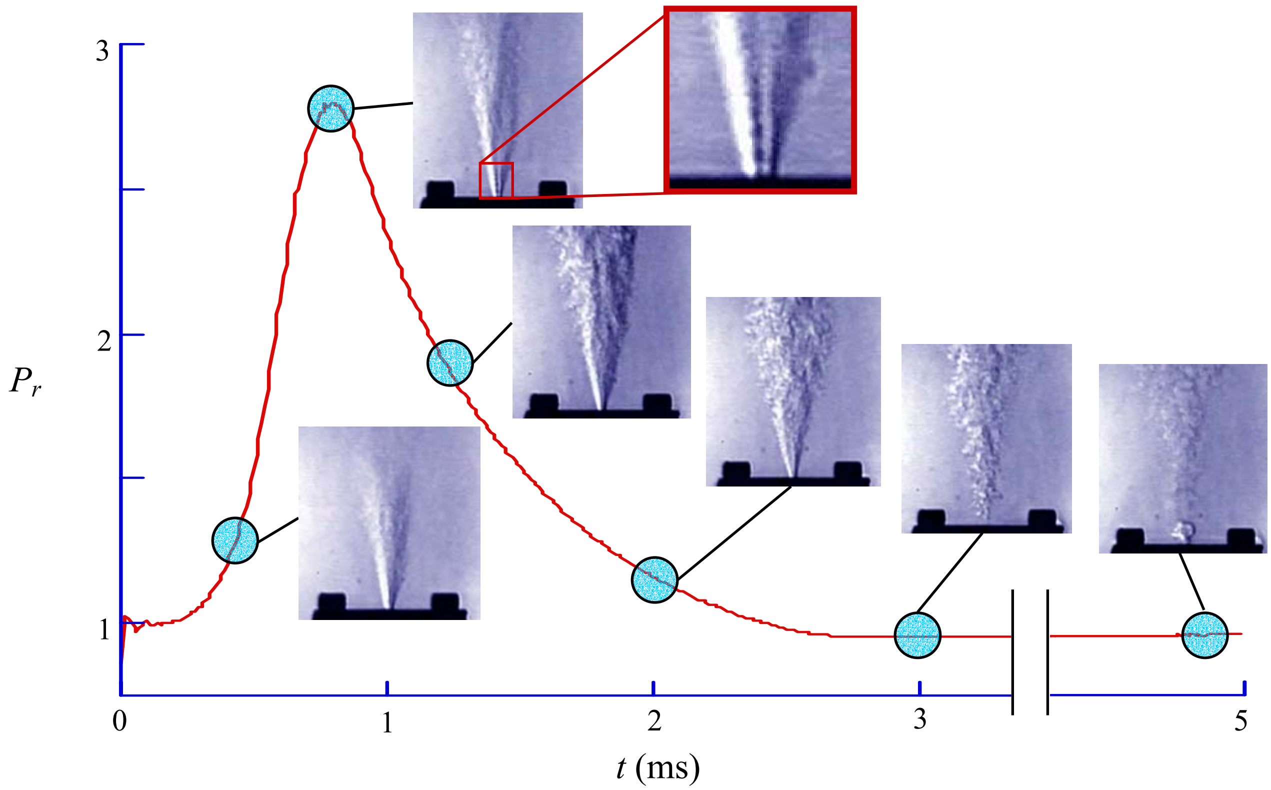

Figure 7. Phase-locked Schlieren images and combustor pressure over single burst for 1 cm^3 volume with 1.30 mm orifice diameter and hydrogen/air ($\Phi = 0.7$) mixture

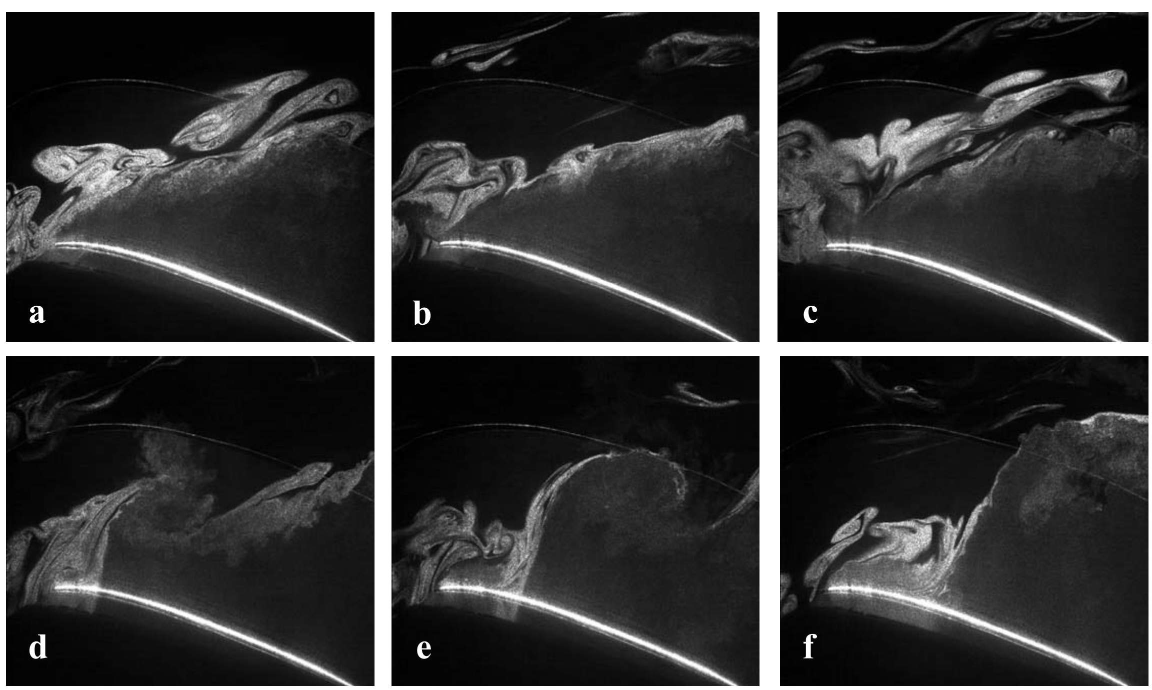

Figure 8. Smoke flow visualization of transient response for actuators in leading edge of unconventional airfoil with $\alpha = 24.1^{\circ}$ and $U_{\infty} = 12.5$ m/s ($Re = 1.95\text{x}10^5$) at t = 0 (a), 1 (b), 3 (c), 8 (d), 12 (e), and 16 (f) ms.

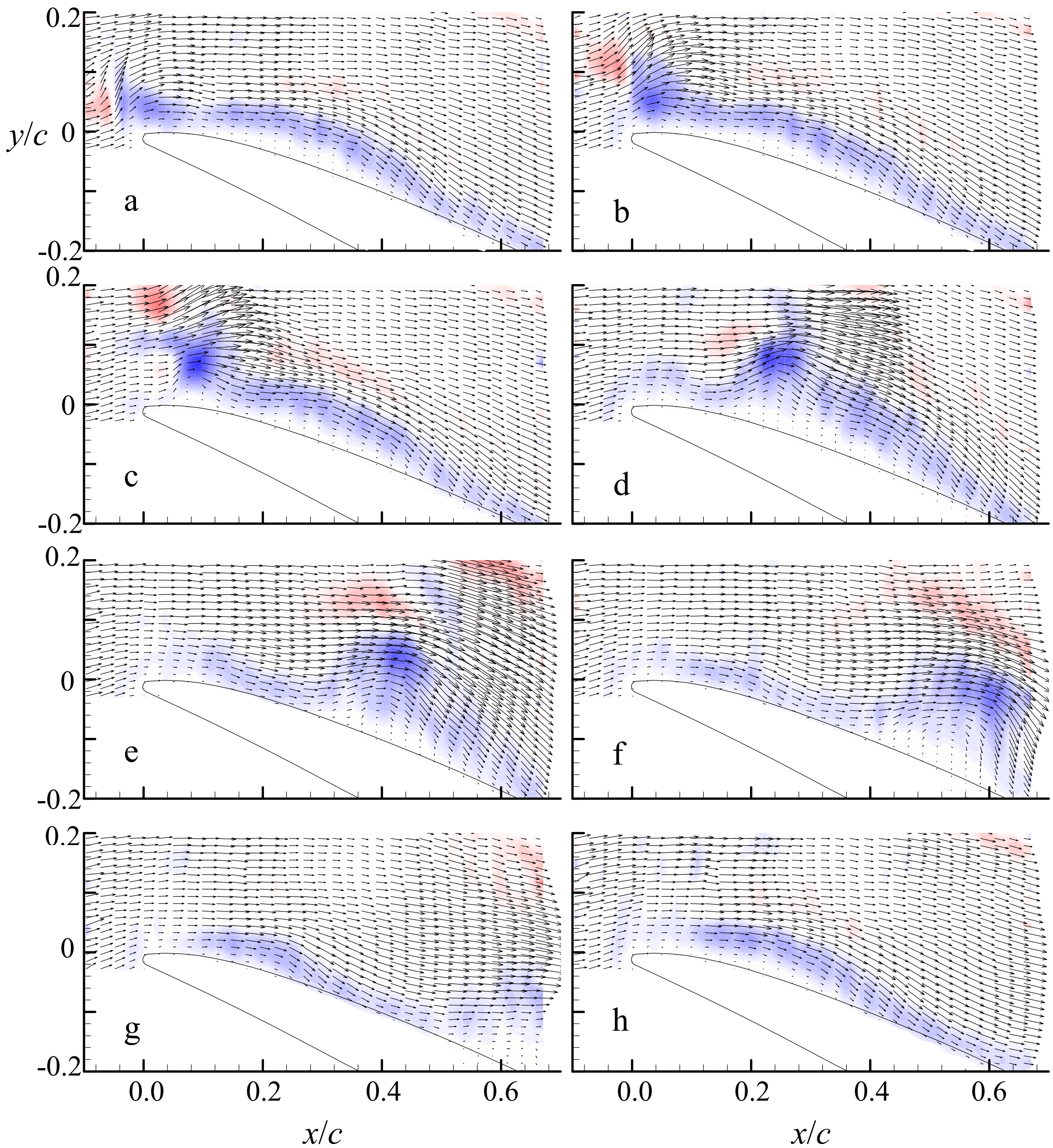

Figure 9. PIV velocity vector fields and vorticity contours for $\alpha = 24.1^{o}$ and U_{∞} = 12.5 m/s with f = 45 Hz (St = 0.82) for t/τ = 0.045 (a), 0.090 (b), 0.135 (c), 0.270 (d), 0.405 (e), 0.540 (f), 0.675 (g), and 0.900 (h).

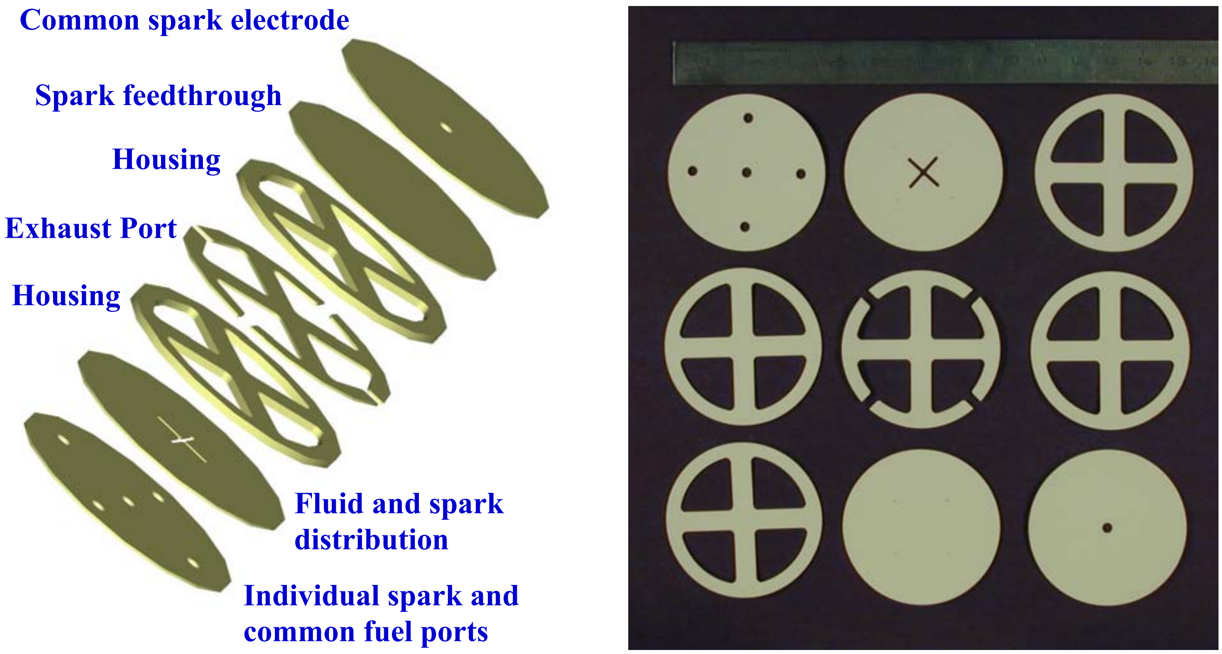

Figure 10. Individual component layers for four actuator array of combustors using laser-cut ceramic laminate sheets.

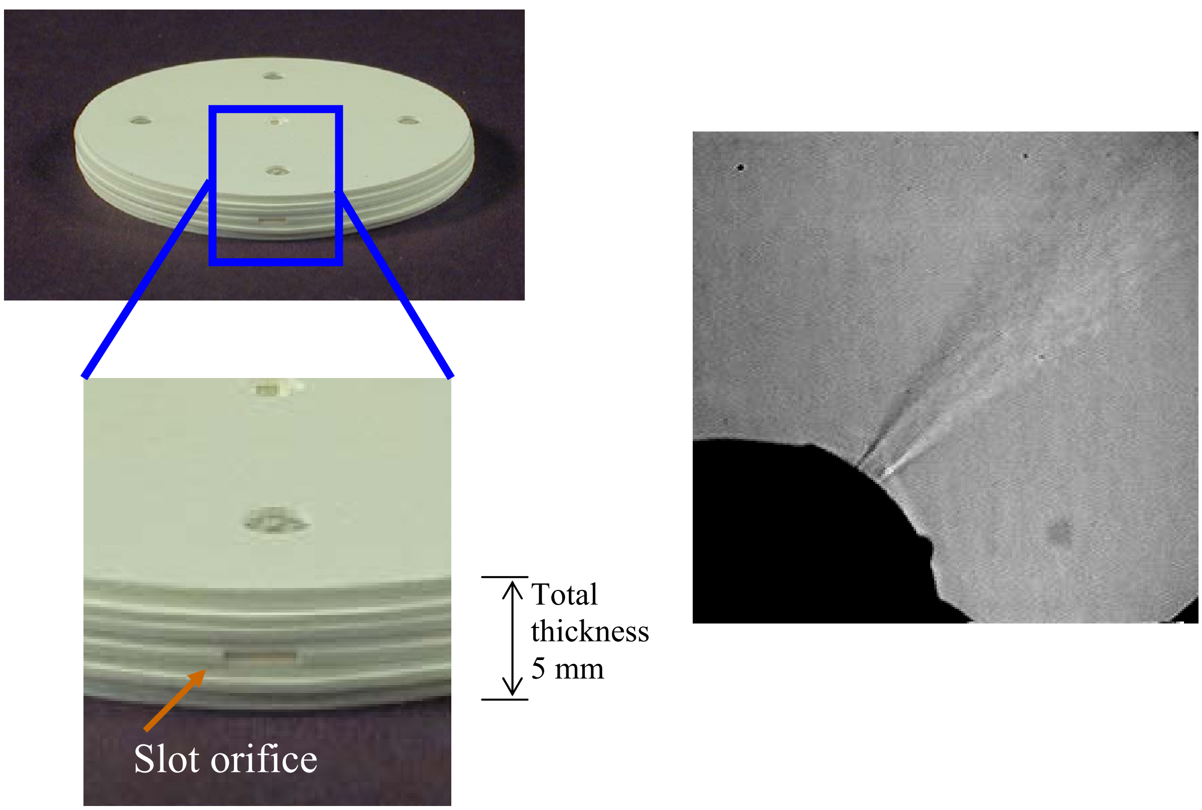

Figure 11. Actuator array after sintering process with Schlieren image of exhaust jet from a single chamber in the array